Archana *et al. Earth, Planets and Space* (2023) 75:122
https://doi.org/10.1186/s40623-023-01874-9

Earth, Planets and Space

FULL PAPER

Open Access

Prompt penetration effects on Equatorial Electrojet from the Indian sector

R. K. Archana[1,2*], Kusumita Arora[1] and Nandini Nagarajan[1]

Abstract

The morphology of prompt penetration effects (PP) in the Equatorial Electrojet (EEJ) at Vencode (VEN, Geomagnetic latitude 0.29ºN) was studied using 5-min samples of EEJ and interplanetary Ey component data from 2011 to 2015. In contrast to previous studies that mainly focused on storm-time PP events, our study investigated the characteristics of PP effects on EEJ during both quiet and disturbed periods. Our findings reaffirm earlier reports of high PP efficiency during local noon for both quiet and disturbed days. Moreover, PP amplitudes were greater when IMF-Bz was oriented northward compared to southward, indicating the presence of overshielding effects even during quiet conditions. Additionally, we examined seasonal variations in PP amplitudes and observed weaker PP during the solstice compared to the equinox. Furthermore, our study analysed the equatorial counter electrojet (CEJ) caused by PP events associated with northward-turning IMF-Bz. We report 15% of CEJs at VEN associated with PP effects; a few PP events were observed while the equatorial electric field at VEN was already westward (i.e. PP within CEJ), indicating the combined effects of magnetospheric and ionospheric perturbations. Identifying CEJs caused by PP during quiet days helps to differentiate between magnetospheric and ionospheric mechanisms/processes. Additionally, we investigated the spatial variability in PP amplitudes at closely spaced sites, utilizing one year of concurrent data from Minicoy (MNC, Geomagnetic latitude 0.19ºN), VEN, and Campbell Bay (CBY, Geomagnetic latitude 0.29ºN) situated at geographic longitudes 72º, 77º and 93º, respectively. Our results showed significant differences in PP amplitudes between VEN-CBY and MNC-CBY, separated by 15º and 20º longitude, respectively. Observations from the three equatorial sites demonstrated a longitudinal trend, with PP amplitudes increasing westward towards MNC, inverse to the amplitudes of EEJ.

Keywords Prompt penetration, Equatorial Electrojet, Counter electrojet

*Correspondence:
R. K. Archana
archanamgp.ngri@gmail.com
Full list of author information is available at the end of the article

Graphical Abstract

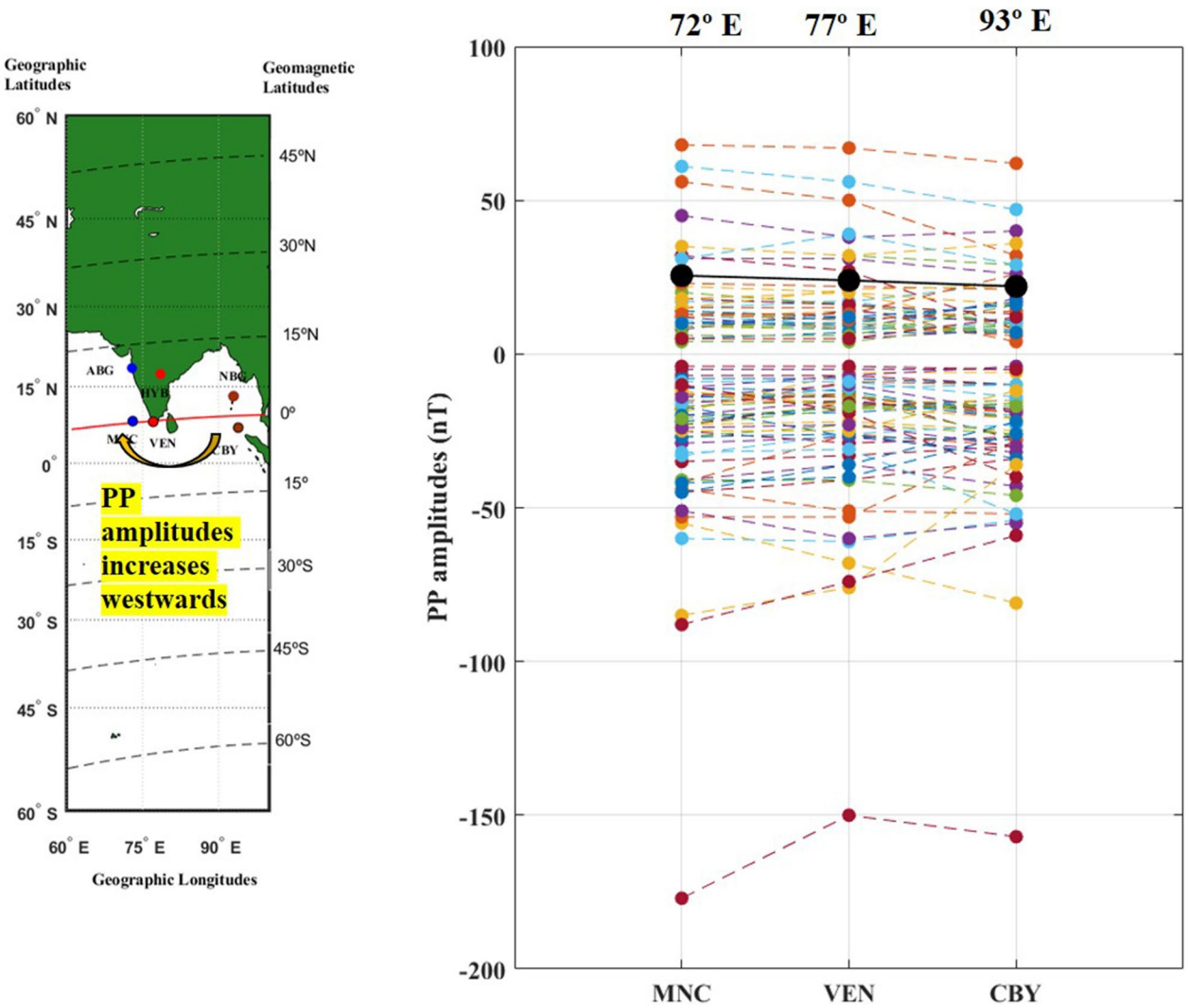

Introduction

Direct penetration of the Interplanetary Electric Field (IEF) through the high-latitude ionosphere into highly conductive equatorial-low latitudes is known as prompt penetration (PP) (Nishida 1966, 1968), which can last from seconds to hours. A significant portion of the variations in the geomagnetic equatorial ionospheric electric field can be attributed to PP effects. Huang et al. (2005) suggested that PP represents the electric field of solar wind/magnetosphere origin, observed equatorward of the shielding layer. PP events are identified as simultaneous fluctuations in the dawn–dusk component of the solar wind-interplanetary electric field (Ey) and the horizontal component of the equatorial-low latitude geomagnetic field (Kelley et al. 1979; Kikuchi et al. 1996; Huang et al. 2005; Nicolls et al. 2007).

Studies suggest that PP fields originate from under-shielding and overshielding conditions, as well as from the divergence of asymmetric ring currents (Ridley and Liemohn 2002; Fejer et al. 2007; Sharma et al. 2011) and increased polar cap potential drop (Fejer et al. 2007; Senior and Blanc 1984). Under-shielding fields are generated when the north–south component of the interplanetary magnetic field (IMF Bz) turns southward with a large value. Conversely, a sudden northward turning of IMF Bz from its steady southward configuration results in the generation of overshielding fields. The under-shielding/overshielding fields exhibit an eastward/westward

orientation during the day and a westward/eastward orientation during the night (Gonzales et al. 1979; Fejer 1986; Fejer and Scherliess 1997).

Jaggi and Wolf (1973) suggested that prompt penetration is the result of a temporary failure of the shielding mechanism. The convection electric field in the outer magnetosphere (R1 region) and the polarized electric field in the ring current region (R2 region) are proposed as the sources of PP and the shielding electric field, respectively. The instantaneous transmission of the polar electric field to the equator is explained by means of TM0 mode waves in the Earth-ionosphere waveguide (Kikuchi et al. 1978; Kikuchi and Araki, 1979; Kikuchi et al. 1996). It is suggested that Region-1 field-aligned currents (R1 FACs) flow into the equatorial ionosphere via the polar ionosphere and are amplified by the Cowling effect. The enhanced conductivity associated with the Equatorial Electrojet (EEJ) facilitates the occurrence of PP events in geomagnetic equatorial latitudes. Earle and Kelley (1987) argue that the shielding effect by the ring current system is effective only for periods greater than 10 h. According to their findings, the magnetosphere can act like a capacitor, allowing fluctuations with periods shorter than 10 h to pass through.

The effects of PP in EEJ during disturbed and quiet conditions have not yet been widely investigated; most studies on PP being confined to storm-time events. Recently, Bulusu et al., (2018, 2020) have detected PP events associated with major and minor storms during 2015 in the Indian sector during main and the recovery phase, and reported PP amplitudes varying longitudinally. In this study, we extract daytime PP signatures at three equatorial sites and evaluate their characteristics over disturbed and quiet conditions, over local time, IMF-Bz direction and longitudinal differences.

Objectives

The characteristics of EEJ and CEJ in the Indian sector have been studied extensively for several decades. Previous research has focused on various aspects such as day-to-day variability, seasonal variations, solar cycle dependence, spatial variability, influence of Sq focus, neutral winds, and geomagnetic storm effects. However, there has been no attempt to specifically identify the influence of interplanetary field disturbances on EEJ during quiet times and its longitudinal variability, which is crucial for accurate modelling of PP effects on EEJ and improving the modelling of space weather effects at equatorial stations.

The current study investigates the morphological characteristics of PP effects on the EEJ during geomagnetically quiet and disturbed periods and across different seasons. Additionally, longitudinal trends of PP effects have been examined.

The focus of the work is listed below:

- Evaluate the influence of local time and IMF-Bz on PP effects during geomagnetic quiet and disturbed conditions.
- Estimate longitudinal variations in PP effects at close spatial separations.
- Identify CEJs caused by PP.

Data and methodology

Geomagnetic horizontal component (H) data sampled at 1-min intervals from the equatorial sites MNC, VEN, CBY, and the low latitude sites ABG, HYB, and NBG have been used to obtain the strength of the Equatorial Electrojet (EEJ) at the respective equatorial sites. The locations of the sites are shown in Fig. 1 and Geomagnetic and Geographic coordinates are provided in Table 1. The 1-min sampled data were converted to 5-min averages

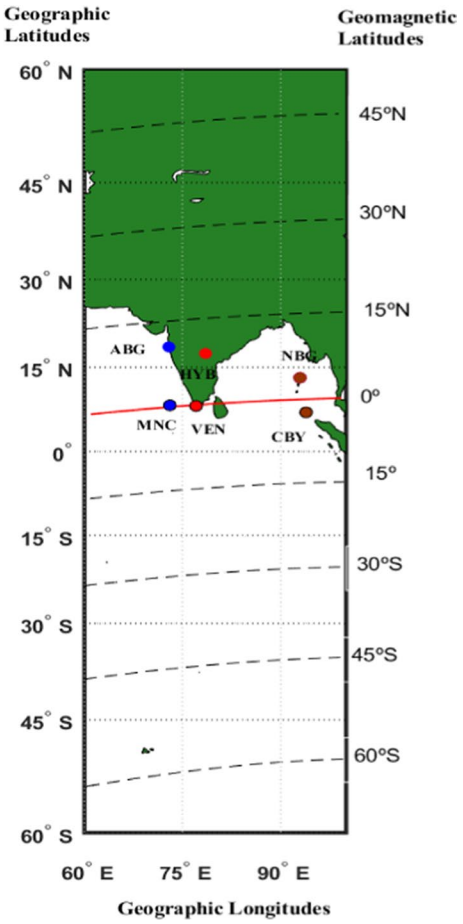

Fig. 1 Location of the sites used in the study

Table 1 Geographic and geomagnetic coordinates of the sites

Sites	Geographic lat	Geographic long	IGRF 2015, 12th generation		
			Geo mag lat	Geo mag long	Inclination 2015
MNC	08.27°N	73.05°E	00.19°N	146.08°E	02.646°
ABG	18.655°N	72.867°E	10.48°N	146.89°E	26.551°
VEN	08.15°N	77.10°E	00.29°N	150.06°E	02.049°
HYB	17.41°N	78.54°E	08.77°N	152.23°E	23.641°
CBY	07.00°N	93.88°E	02.47°S	166.59°E	− 01.584°
NBG	13.16°N	92.95°E	03.68°N	165.93°E	13.397°

and diurnal variations of H (ΔH) were obtained by subtracting the midnight means of H (00:00, 01:00, 22:00, and 23:00) Local Time (LT) hours, which are assumed to represent the main and crustal contributions. The ΔH values at the equatorial sites MNC, VEN, and CBY represent the combined EEJ and Sq (Solar quiet) variations at those longitudes, while the ΔH values at the low latitude sites ABG, HYB, and NBG represent the Sq component at their respective longitudes. The differences in ΔH between the equatorial and low latitude sites within the same longitudinal sector provide the strength of the EEJ. The amplitudes of Sq at NBG have been normalized to ABG/HYB level by doing a latitudinal correction explained in Archana et al. 2018.

The EEJ values at 5-min sampling intervals were calculated at VEN for the period 2011–2015 and at MNC and CBY for the year 2015 using the above method. The interplanetary electric field (Ey) data in geocentric solar magnetic (GSM) coordinate system used here were downloaded from the OMNI website using the following link: https://omniweb.gsfc.nasa.gov/ow_min.html. The Ey component is the product of the horizontal component of the solar wind velocity and the vertical component of the interplanetary electric field, as given in the equation below:

$$\mathrm{Ey} = -Vx * \mathrm{Bz}.$$

From this equation, it can be noted that Ey and Bz are opposite in direction, i.e. whenever IMF-Bz is south (−ve)/north (+ve) Ey component is in eastward (+ve)/westward (−ve).

Identification of PP

Prompt penetration (PP) events in the Equatorial Electrojet (EEJ) are identified using the method suggested by Bulusu et al. (2018, 2020). The method involves calculating the correlation coefficient between EEJ strength and the Ey component every hour with 90% data overlap during the period 00–12 UT, corresponding to daylight hours in the Indian region. Since the EEJ and Ey are sampled every 5 min, there will be 12 data points within one hour. The first correlation coefficient is calculated between the EEJ and Ey component (12 values each) from 00:00 UT to 01:00 UT, the second correlation is calculated from 00:05 UT to 01:05 UT, and the third correlation coefficient is calculated from 00:10 UT to 01:10 UT. If the calculated correlation coefficient is above 0.7 for three consecutive hours (e.g. 00:00 to 01:00 UT, 00:05 to 01:05 UT, and 00:10 to 01:10 UT) with a threshold change in EEJ amplitude in the range of −/+4 nT and Ey in the range of ± 1 mV/m, it is considered a PP event. The change in the strength of the EEJ during the PP event, represented by simultaneous fluctuations in the EEJ and Ey, is considered the PP amplitude.

The threshold values for the EEJ and Ey are defined to minimize possible false positives. Bhaskar et al. (2013) selected PP events where the IMF-Bz and EEJ exhibited a sharp threshold change of ± 3 nT and ± 7 nT, respectively. The estimated Ey corresponding to a ± 3 nT variations in IMF-Bz with averaged solar wind velocity is ± 1.3 mV/m. In our present study, we are examining PP effects during both quiet and disturbed times in the EEJ; hence, the threshold for Ey and EEJ has been lowered to ± 1 mV/m and ± 4 nT, respectively.

In order to determine the statistical significance of the correlation coefficient calculated at each one-hour interval, which is based on the 12 values (degrees of freedom) of the EEJ and Ey components, a P and T test was conducted. This test helps establish whether a correlation coefficient of 0.7 represents a "good correlation".

The formula for the T-test is,

$$t = \frac{r\left(\sqrt{n} - 2\right)}{\left(\sqrt{1} - r^2\right)},$$

where 'r' represents the obtained correlation coefficient and 'n' denotes the number of degrees of freedom. The calculated T values are then compared with the T value from the statistical table (Kpkoska and Nevison 1989) for (n−1) degrees of freedom. If the calculated T values are higher than the T value from the statistical table, it

confirms that the correlation coefficient is statistically significant. In the present study, with 12 data points, the *T* value from the table is 1.7823. Additionally, the p-value is computed using a t-distribution with (n−2) degrees of freedom. The proximity of the *p*-values to zero indicates the statistical significance of the computed correlation coefficients.

An example for the identification of PP events on a quiet day is provided in Fig. 2a–c. The figure displays the 5-min sampled Ey and EEJ data from VEN on 10th December 2011, which is a quiet day (Fig. 2a), and b presents the corresponding correlation coefficient (CC), *P*-test values, calculated *T*-test values, and the *T*-value obtained from the statistical *T*-table. Figure 2c shows the geomagnetic indices Kp*10 and Dst for the same day.

From Fig. 2b, it is evident that during the 05–06 UT period, the calculated correlation coefficient remains consistently above 0.7, with the highest CC value being 0.96. The amplitude changes in EEJ (ΔEEJ, i.e. PP amplitude) during this event are 25 nT, while in Ey (ΔEy), it is 2 mV/m, higher than the threshold amplitudes. Therefore, this event is identified as a PP event, as indicated by the dashed rectangle in the figure. The calculated *T*-values are greater than the *T*-value from the table, and the *P*-values are approximately 0, confirming that the observed correlation coefficient during the event is statistically significant.

From Fig. 2c, it can be observed that the maximum Kp10 value on the given day is 20, and the minimum Dst value is − 28 nT, confirming that 10th December 2011 is a geomagnetically quiet day. During the observed PP event (05–06 UT), the Kp10 index is 20, and the Dst index ranges from − 2 to − 10 nT indicating the geomagnetic quiet time condition.

Another example of PP identification during a disturbed day is shown in Fig. 2d–f for 5th February 2011. From the figure, it is evident that there is a clear correspondence between the oscillation in EEJ and Ey during the 05–07 UT period, with the correlation coefficient (CC) consistently greater than 0.7 and a maximum value of 0.97. The *P*-values are close to zero, and the calculated *T*-values are higher than the *T*-values from the statistical table, confirming the statistical significance of the correlation coefficient. During this period, the amplitude change in EEJ (ΔEEJ) is − 28 nT, and in Ey (ΔEy), it is − 5 mV/m, indicating a PP event. The Kp*10 and Dst indices during the observed PP event are 38 and − 50 nT, respectively, which further indicate geomagnetic disturbances. Figure (2a–f) confirms that this method is suitable for identifying PP events during both quiet and disturbed periods.

Observation and results

Based on observations from five years of data at VEN (2011–2015) and one year of data analysis at MNC and CBY (2015), the statistics of PP events at these sites are provided in Table 2. A total of 321 PP events were identified at VEN during 2011–2015, with 136 events observed during quiet times and 185 events observed during disturbed times. This illustrates that not all PP events are associated with storms or large disturbances, and interplanetary effects can be observed in the equatorial ionosphere even during quiet days. The table also indicates that on several days, Ey has shown significant amplitude variations, but not all of

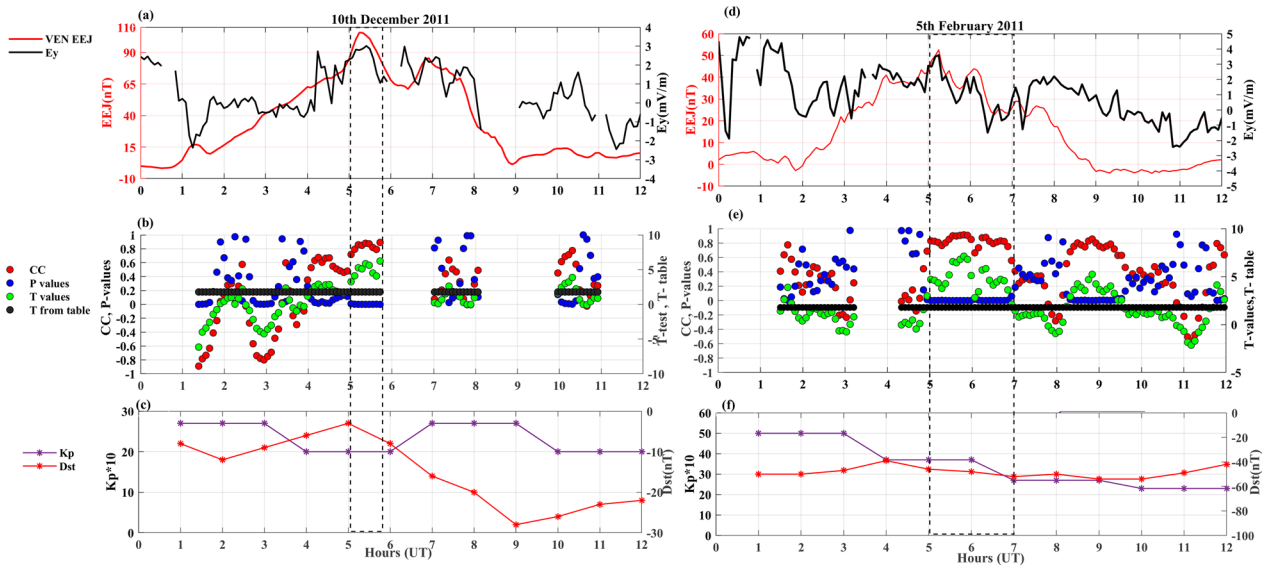

Fig. 2 Sample plot of five-minute averaged EEJ at VEN and Ey on 10th December 2011 (**a**); calculated Correlation coefficient (CC), P and Test values, and T- from T- table for each hour (**b**). The hourly Kp index*10 and Dst values (**c**); a dashed rectangle has highlighted the PP event

Table 2 The statistics of occurrence of PP events

	Year	Total days	PP days	Days with No Ey fluctuations	Days with Ey variations and No PP	PP when Kp*10 < 30	PP when Kp*10 > 30
VEN	2011	228	29	5	194	23	6
	2012	241	58	29	156	28	29
	2013	335	77	45	218	36	36
	2014	184	48	19	118	42	6
	2015	290	109	17	169	50	54
	Total	1270	321	115	855	130	180
CBY	2015	231	97	12	111	35	62
MNC	2015	290	104	17	169	36	68

them resulted in PP events. Currently, there are no explanations for this phenomenon. Furthermore, a similar number of total PP events observed at the three equatorial sites in 2015 suggests that PP events are simultaneously observed at these sites.

Occurrence of PP events with solar cycle

The occurrence pattern of PP during different phases of solar cycle-24 is investigated by plotting the percentage of PP event occurrences at VEN during 2011–2015, along with the annual means of sunspot numbers and F10.7, as shown in Fig. 3a. The figure also displays the total number of days used in each year and the total number of identified PP events, as depicted in Fig. 3b. Additionally, the observed PP events are categorized according to the Kp*10 index, as illustrated in Fig. 3c.

From the figure, it can be observed that the number of PP events increases with solar activity. The lowest occurrence of PP events (12% of occurrences) was observed in 2011, while the highest occurrences of PP events were in 2015 (35% of occurrences). The relationship between PP occurrence and solar activity is not linear. Despite high solar activity in 2014 based on F10.7 and sunspot numbers, the occurrence of PP events was only 26%. In contrast, there is not a significant difference in solar activity between 2011 and 2012, yet the PP occurrence in 2012 is around 23%, compared to 12% in 2011. Except for 2011 and 2014, the observed PP events are almost equally distributed between quiet time events and disturbed time events. In 2011 and 2014, the number of storms (Dst < − 50) is around 12, whereas in all other years, the number of storms is more than 20. The increased geomagnetic activity could be the reason for the increase in

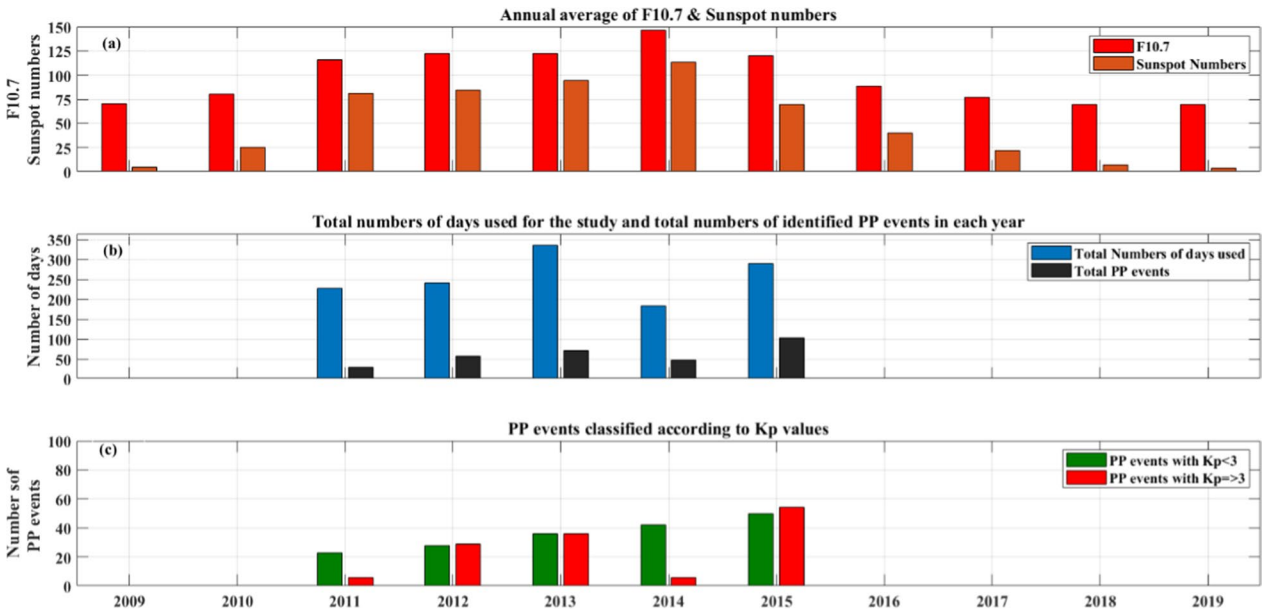

Fig. 3 Annual means of F10.7 and sunspot numbers (**a**); percentage of occurrences of PP in each year (**b**); PP classified according to Kp index

the number of PP events in 2012, 2013, and 2015. However, to establish trends and understand their causes, data over more solar cycles are needed.

Seasonal effects on PP amplitudes

Seasonal effects on PP amplitudes have been investigated using five years of PP observations from VEN. The scatter plots of PP and Ey amplitudes for each season are presented in Fig. 4a, b. PP events are classified based on their Kp*10 index and categorized into four seasons: Winter (DEC–JAN–FEB), Spring Equinox (MAR–APR–MAY), Summer (JUN–JUL–AUG), and Autumn Equinox (SEP–OCT–NOV). Figure 4a examines the seasonal effects on the response of PP to Ey under geomagnetic quiet time conditions, while Fig. 4b demonstrates the response of PP to Ey in each season during disturbed conditions. The figure itself provides the slope of the fitted line for each season. The slope of the fitted line indicates how the PP amplitudes vary with changes in Ey; a higher slope suggests that the response of PP is strongly modulated by Ey amplitudes. From the figure higher slope of the fitted lines indicates that PP efficiency is higher for equinox seasons during quiet conditions compared to solstice season, whereas for disturbed condition such seasonal pattern is not evident.

Influence of local time and IMF Bz turning on PP

To investigate the effects of local time and IMF-Bz direction on PP, the observed PP events at VEN from 2011 to 2015 were classified based on the Kp*10 index and further categorized according to IMF-Bz directions (North and South) and time of occurrence, as depicted in Fig. 5a, b. The amplitudes of PP and corresponding Ey were recorded for all events and then grouped based on their time of occurrence into three categories: morning (00.5–04.5 UT h, i.e. 06–10 LT), noon (04.5–07.5 UT h, i.e. 10–13 LT), and afternoon/evening (07.5–12.5 UT h, i.e. 13–18 LT). Due to the low number of PP events observed during the evening hours, they were combined with the afternoon events.

Figure 5a presents the amplitudes of PP and Ey during geomagnetically quiet conditions at different local times for both IMF-Bz north and south. The figure consistently demonstrates that the slope for IMF-Bz north is greater than that for IMF-Bz south, regardless of the time of occurrence. The steepest slope is observed during local noontime for both IMF-Bz north and south. Specifically, during local noontime, the slope between PP and Ey is 3.9 for IMF-Bz north and 2.4 for IMF-Bz south. The range of PP amplitude variations during local noontime is − 4 to − 60 nT for IMF-Bz north orientation, while for IMF-Bz

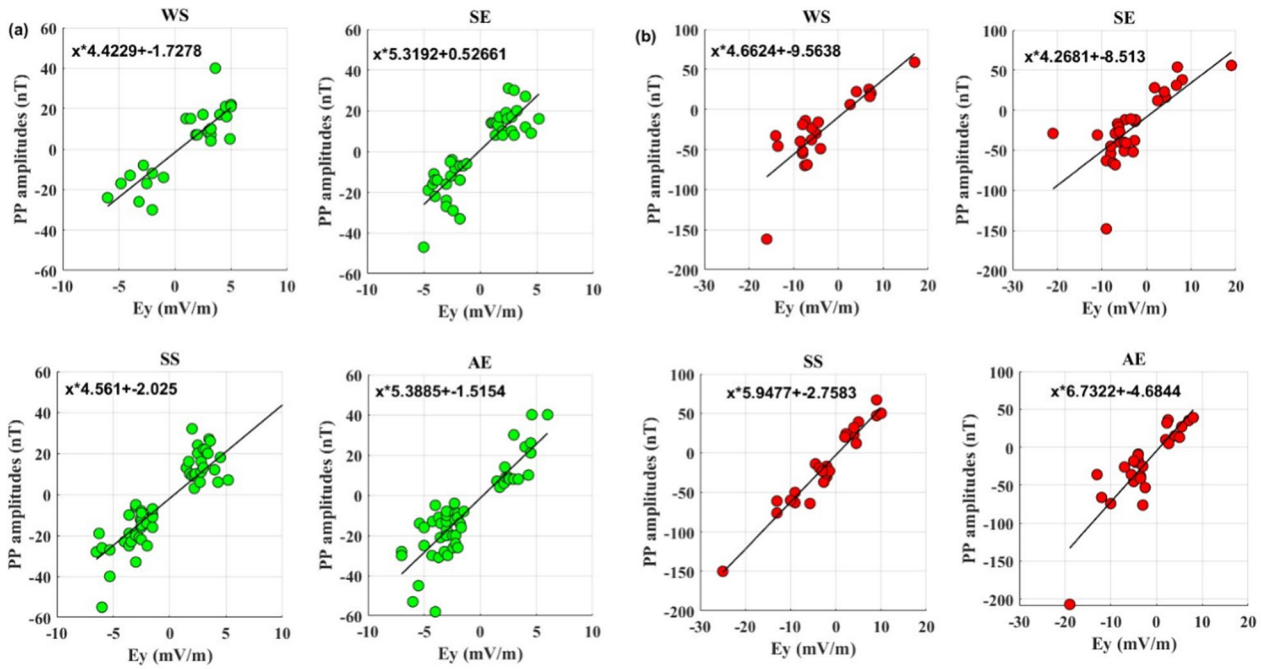

Fig. 4 **a** PP amplitudes at VEN and Ey amplitudes for different seasons for all days with Kp*10 < 30. WS-Winter Solstice; SE-Spring Equinox; SS-Summer Solstice; AE-Autumn Equinox. **b** PP amplitudes at VEN and Ey amplitudes for different seasons for all days with Kp*10 ≥ 30; *WS* winter solstice, *SE* spring equinox, *SS* Summer solstice, AE autumn equinox

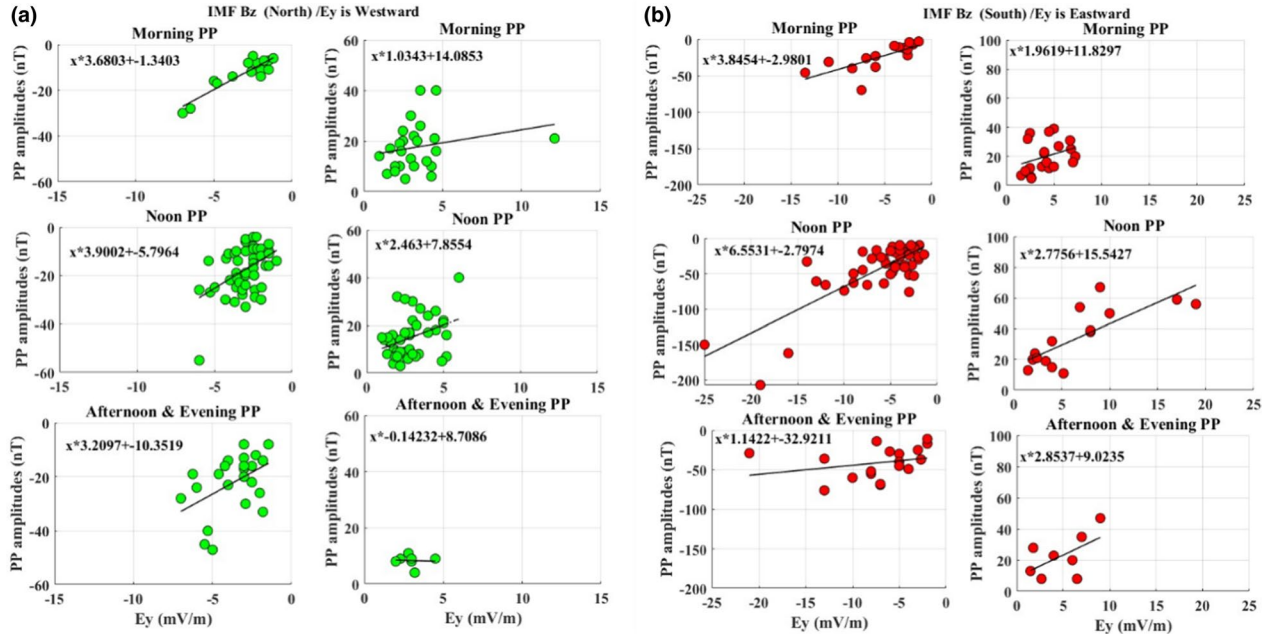

Fig. 5 **a** The amplitude variation in EEJ and Ey component corresponding to the occurrences of PP events identified for Kp*10 < 30 days classified according to the direction of Ey/IMF- Bz and further according to the time of occurrences. **b** The amplitude variation in EEJ and Ey component corresponding to the occurrences of PP events identified for Kp*10 > 30 days classified according to the direction of Ey/IMF- Bz and further according to the time of occurrences

south orientation, it is 4 to 40 nT, for the same range of Ey amplitude variations of ± 1 to ± 7 mV/m.

Fig. 5b provides a similar analysis to Fig. 5a but focuses on disturbed periods (Kp*10 ≥ 30). During disturbed times, the range of PP amplitudes expands to − 200 to 65 nT, and the variations in Ey range from approximately ± 20 to ± 7 mV/m. When examining the influence of IMF-Bz orientations, it is observed that for northward IMF-Bz, the range of PP is − 4 to 200 nT, whereas for southward IMF-Bz, it is 4 to 65 nT, considering the Ey ranges from ± 1 to ± 20 mV/m. Figure 5a, b confirms that the efficiency of PP is higher for local noon-time hours and for IMF-Bz north orientation for both quiet and disturbed time.

Longitudinal variation in PP amplitudes

The study further investigated the longitudinal variations in PP using concurrent geomagnetic data from MNC (72°E), VEN (77 °E), and CBY (93 °E) during 2015, where MNC-VEN is separated by 5°, VEN-CBY is separated by 15°, and MNC-CBY is separated by 20° longitudes. The PP events at these sites were categorized as either quiet or disturbed events based on the Kp*10 values presented in Fig. 6. Figure 6a represents the quiet time PP amplitude at the sites and Fig. 6b represents disturbed time events. These include the PP events from all storms that occurred in 2015. Interestingly, for both quiet and disturbed PP events, there is an overall pattern indicating an increase in PP amplitudes towards MNC.

Further, the absolute differences in PP amplitudes between pairs of sites for all events in 2015 are shown in Fig. 7. The positive differences in PP amplitudes between sites, such as $\left|\text{MNC}\right| - \left|\text{VEN}\right|$, indicate that PP amplitudes at MNC are greater than at VEN, while negative values indicate that VEN has greater amplitudes than MNC. The blue shaded portion in Fig. 7 indicates an increase in PP amplitudes towards the west, i.e. at MNC for the pair $\left|\text{MNC}\right| - \left|\text{VEN}\right|$, at VEN for the pair $\left|\text{VEN}\right| - \left|\text{CBY}\right|$, and at MNC for the pair $\left|\text{MNC}\right| - \left|\text{CBY}\right|$. The events in the shadeless portion indicate PP events with higher amplitudes towards CBY.

The main observations from Fig. 7 are as follows: the difference in PP amplitudes increases with longitudinal separations. At 5° longitudinal separations (i.e. between MNC-VEN), the difference in PP amplitudes lies within ± 5 nT for more than 65% of the events. At 15° (VEN-CBY) and 20° (MNC-CBY) longitudinal separations, PP amplitudes between the sites shows a difference that exceed ± 5 nT for the majority (~ 65%) of events. At 20° longitudinal separations, many events exhibit significant difference in PP amplitude greater than ± 15 nT.

Figure 8a–c provides examples of longitudinal variations in PP amplitudes. Figure 8a represents a PP event

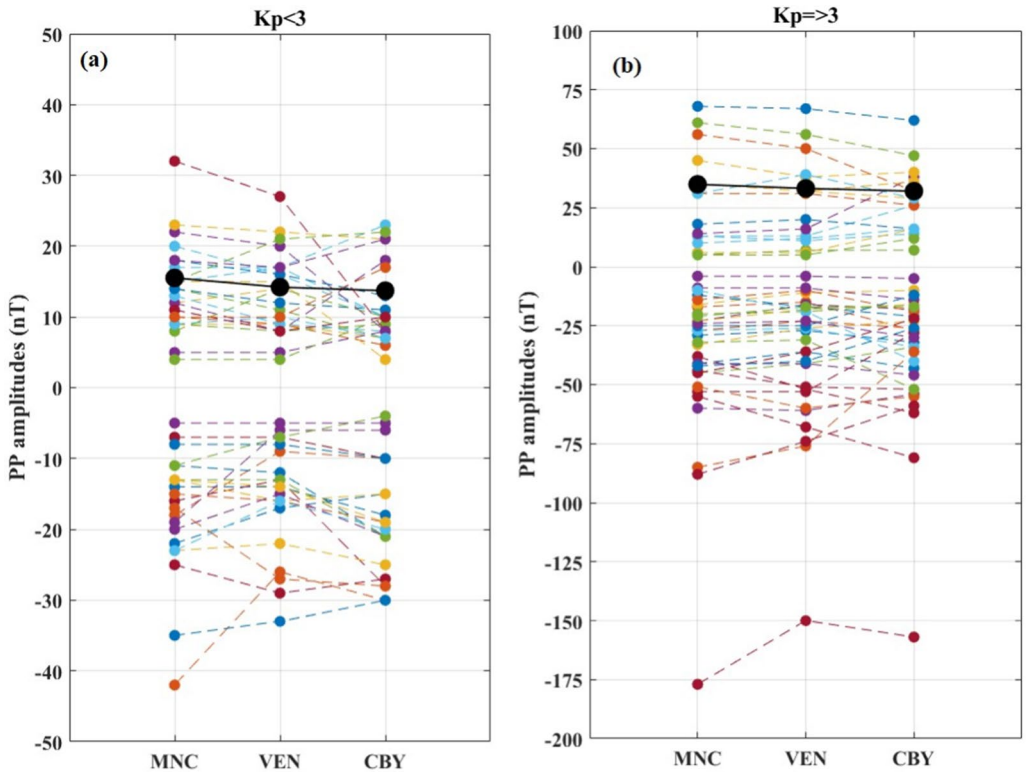

Fig. 6 The amplitudes of all quiet time PP events from 2015 at MNC, VEN and CBY (**a**) and disturbed time (**b**). The black big balls indicate the mean of absolute PP amplitudes at each site

that occurred during a quiet time on June 18th, 2015. The Kp*10 value during the event was 27, indicating a geomagnetically quiet condition. A sudden change in Ey from east to west with an amplitude change of − 1.5 mV/m around 3.5 UT resulted in a sharp decrease in the Equatorial Electrojet (EEJ) at all three sites. This led to PP events with amplitudes of − 11 nT at MNC, − 7 nT at VEN, and − 4 nT at CBY.

Figure 8b presents an example of longitudinal variation in PP during disturbed time on May 19th, 2015 (Kp*10 = 50). Around 03:10 UT, a sudden decrease in Ey (− 12 mV/m) was observed, causing a depression in the EEJ at all three sites. The PP amplitudes during this event were − 34 nT at MNC, − 31 nT at VEN, and − 52 nT at CBY. Prior to the occurrence of PP (02:30 UT), the EEJ strength was 17 nT at MNC and VEN, and 47 nT at CBY, indicating the ionization levels at the respective sites. It can be observed from the figure that PP resulted in a Counter Electrojet (CEJ) with amplitudes of − 18 nT at MNC, − 15 nT at VEN, and − 5 nT at CBY. As the EEJ strength at MNC and VEN was already weak compared to CBY, it was relatively easier to bring the EEJ strength below the night level and result in a CEJ.

Another example is provided in Fig. 8c for a disturbed time, with a Kp*10 value of 53 at the time of the PP occurrences. PP was observed at all three sites during 07:00–10:00 UT, with extremely high amplitudes at MNC (− 98 nT) and VEN (− 89 nT) compared to CBY (− 45 nT). The ΔEy for this event was − 15 mV/m. The amplitudes of the EEJ just before the PP events were 18 nT at MNC and VEN, whereas 38 nT at CBY. The PP events at MNC and VEN resulted in a negative depression of the EEJ, leading to CEJs. The amplitudes of the CEJs were − 78 nT at MNC, − 75 nT at VEN, and − 5 nT at CBY. Figure 8b, c demonstrates that PP can result in CEJs, and the amplitudes of the CEJs vary with longitudes.

CEJ and PP

An attempt has been made to identify CEJs at VEN caused by PP during quiet time. The individual examples of CEJs caused by PP during a quiet day are shown in Fig. 9a, b. On February 20th, 2013 around 09:30 UT, a CEJ with an amplitude of − 12 nT observed at VEN (around 15:00 LT) and CEJ of amplitude − 3 nT noted at CBY (around 16:00 LT), the corresponding Ey fluctuation was − 2 mV/m (Fig. 9a). The figure confirms that this CEJ

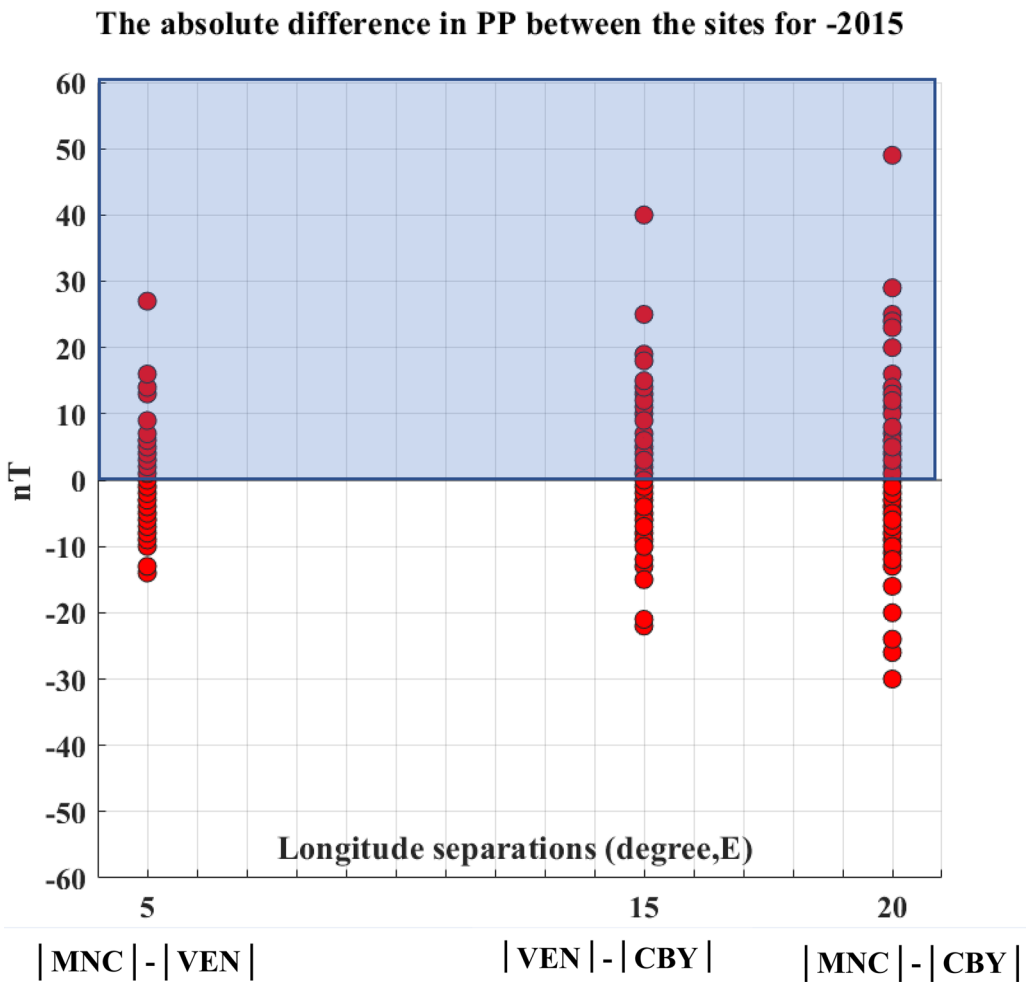

Fig. 7 The difference in absolute PP amplitudes between the site for 2015 is shown for MNC-VEN; VEN-CBY and for MNC-CBY pairs, which are separated at 5º, 15º and 20º longitudes, respectively

clearly has an interplanetary/magnetospheric origin, and the response at the two sites demonstrates the modulating influence of local time on ionization intensity. The amplitude of CEJ is higher at VEN than at CBY due to differences in ionization intensity caused by differences in the local time. A morning CEJ (01–02 UT) was also observed only at VEN with an amplitude of – 8 nT, but Ey data were missing, and PP could not be identified.

An example of the combined signature of ionospheric and interplanetary effects (highlighted by the dashed rectangle) is shown in Fig. 9b. PP is observed within the CEJ at VEN on April 26th, 2013 (Kp*10 = 30). A morning CEJ with an amplitude of – 15 nT is observed at VEN, and a sudden fluctuation in the Ey component (– 2 mV/m) is reflected in the CEJ at the site as a sharp change (– 5 nT) around 2:40 UT. A similar sharp fluctuation is also observed at CBY (– 8 nT) where the CEJ is absent. On the same day (April 26th, 2013) around 04:00 UT, a sharp depression in Ey with an amplitude of – 7 mV/m is observed, which reduces the EEJ strength at the sites and results in a partial CEJ during the noon hours. The amplitude of PP is – 50 nT at CBY and – 20 nT at VEN. Another depression in the EEJ at both sites can be observed between 06 and 07 UT (Fig. 9b), which shows the opposite polarity to Ey. This depression may be of ionospheric or magnetospheric origin.

Figure 10 provides statistics on the total number of PP events. The black bars represent the total number of observed PP events, as well as the number of events where a change in ΔE (± 1 mV/m) occurred but no PP was observed. The ash bars represent the number of CEJs that do not correlate with Ey (816 events) and the number of CEJs that do correlate with Ey (133 events). Based on these statistics, it can be concluded that 15% of the CEJs observed at VEN are caused by PP, indicating interplanetary effects. Additionally, 8% of the observed CEJs

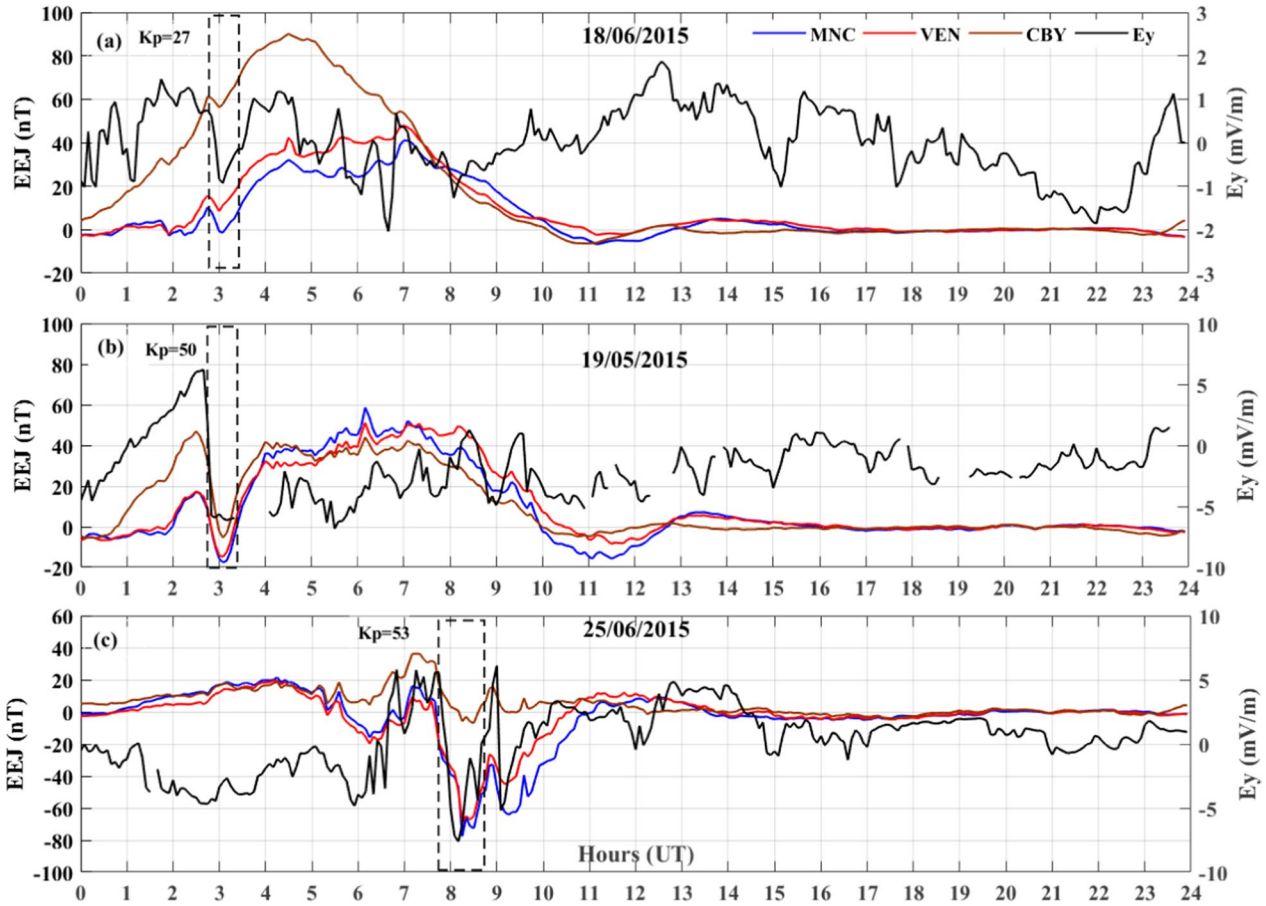

Fig. 8 Five-minute sampled EsEJ and Ey at MNC, VEN and CBY on **a** 18th June 2015, **b** 19th May 2015 and on **c** 25th June 2015, identified PP events are highlighted by dashed black rectangle

show combined signatures of ionospheric and magnetospheric effects. The majority of the observed CEJs at VEN (85%) during the study period do not match with Ey, suggesting the dominance of mechanisms of ionospheric origin rather than interplanetary effects.

Discussion

The present study investigated the characteristics of prompt penetration (PP) effects on the Equatorial Electrojet (EEJ) and Counter Electrojet (CEJ) in the Indian sector during both quiet and disturbed conditions using five years of data. The study also aimed to differentiate the CEJs based on their causal mechanisms as either ionospheric or magnetospheric in origin. Additionally, the study examined the longitudinal variability in PP at close spatial separations. The present work used the novel method of identifying PP suggested by Bulusu et al. (2018, 2020), and our observations indicate that the method is robust even in the identification of PP events observed during quiet time, where the amplitudes are relatively weak (Figs. 2a, 9a).

Further, the analysis of seasonal variations in PP from Fig. 4 shows the highest slope for the equinoxes and the lowest for the solstices. The changes in the slopes of the fitted lines indicate that the response of PP to Ey might be influenced by seasons as the ionospheric conductivity varies with the seasons. The lowest slope in winter indicates that the amplitude variation in PP with Ey is weak in this season compared to others, which could be due to the low ionization and conductivity of the ionosphere. The higher slope observed in the equinox season might be because the Equatorial Electrojet (EEJ) is strongest during this time, possibly amplifying PP events due to higher conductivity and ionization. In the present study, no distinct seasonal effect is evident for disturbed conditions. Figure 4b shows that the highest slope is observed for the autumn equinox and summer solstice, and the lowest slope is observed for the spring equinox. The slope of the fitted line for the winter solstice is higher than that for the spring equinox. There is

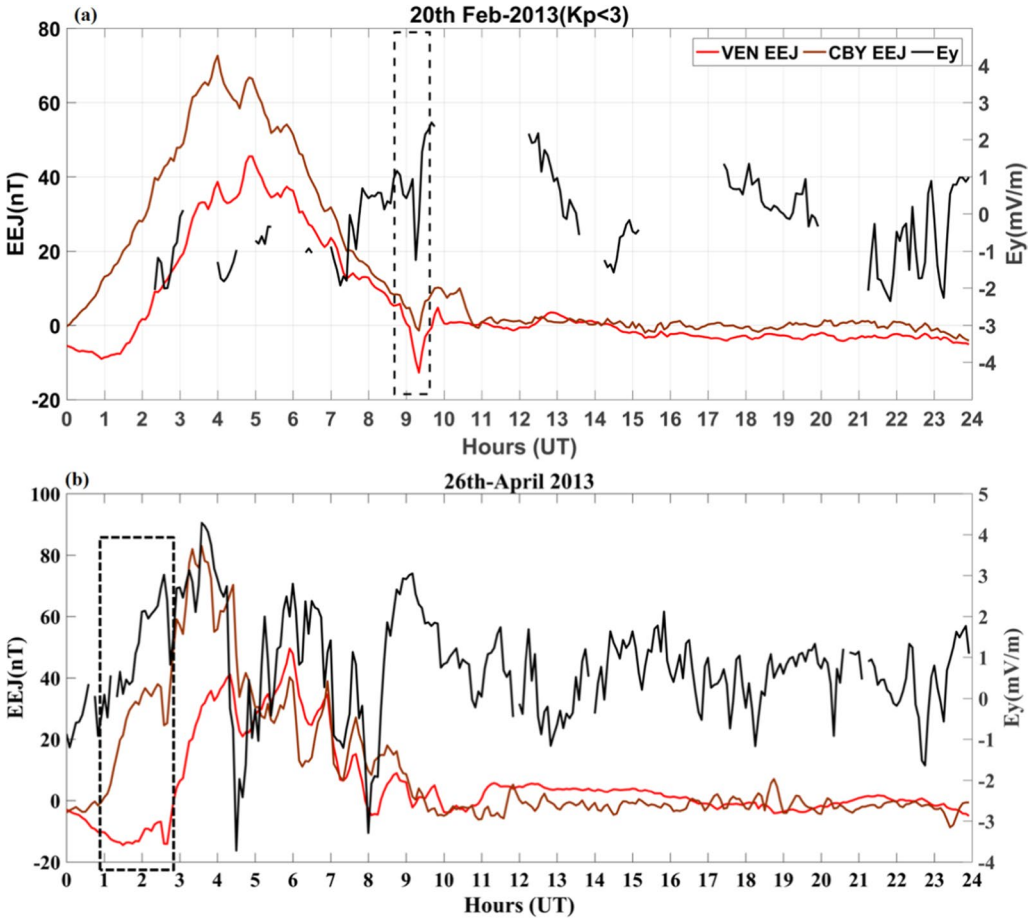

Fig. 9 **a** Ey component and EEJ strength from VEN and CBY on 20th Feb, 2013; the dashed black rectangle indicates the Equatorial counter Electrojet caused (CEJ) by PP; the amplitude of CEJ at VEN is nearly − 13nT; at CBY PP does not cause CEJ instead give rise to a small depression

currently no available literature on the seasonal variability of PP amplitudes.

Figure 5 shows the amplitude of PP and Ey for different times of occurrence during quiet time for both IMF-Bz south and north. The fitted line and its slope indicate the response of PP to Ey amplitudes. The slope of the fitted line is higher for local noon time events compared to morning and afternoon events for both IMF-Bz north and south directions. This could be due to the high ionospheric conductivity caused by large ionization during local noon time, as suggested by Manoj et al. (2008); Bhaskar et al. (2013); Xiong et al. (2016) and Mene et al. (2011).

The efficiency of PP driven by IMF-Bz has been discussed in studies of Equatorial Electrodynamics. Manoj et al. (2008) suggest that PP is independent of IMF-Bz turning, while Bhaskar et al. (2013), Anderson et al. (2002), Kelley et al. (1979), Kikuchi et al. (2000, 2003), and Tsurutani et al. (2008) report that PP efficiency is higher during IMF-Bz northward turning. In this study, we also find that the efficiency is higher during IMF-Bz northward turning, both on disturbed days and quiet days for all local times (Fig. 5). This could be due to the presence of R2-region current overshielding effects, as explained by Jaggi and Wolf (1973) and our study indicates that the overshielding effects due to R2 region currents are effective even during geomagnetically quiet conditions.

There have been few studies so far discussing the longitudinal variation of PP. Mene et al. (2011) have established significant latitudinal, local time, and longitudinal variations of DP2 currents associated with the prompt penetration electric field and reported a significant longitudinal variation in DP2 between African, American and Asian sectors. Using concurrent data sets from MNC, VEN, and CBY during 2015, as well as VEN and CBY during (2012–2013 and 2015), we have studied the longitudinal differences in PP at close spatial separations. All the PP events are simultaneous

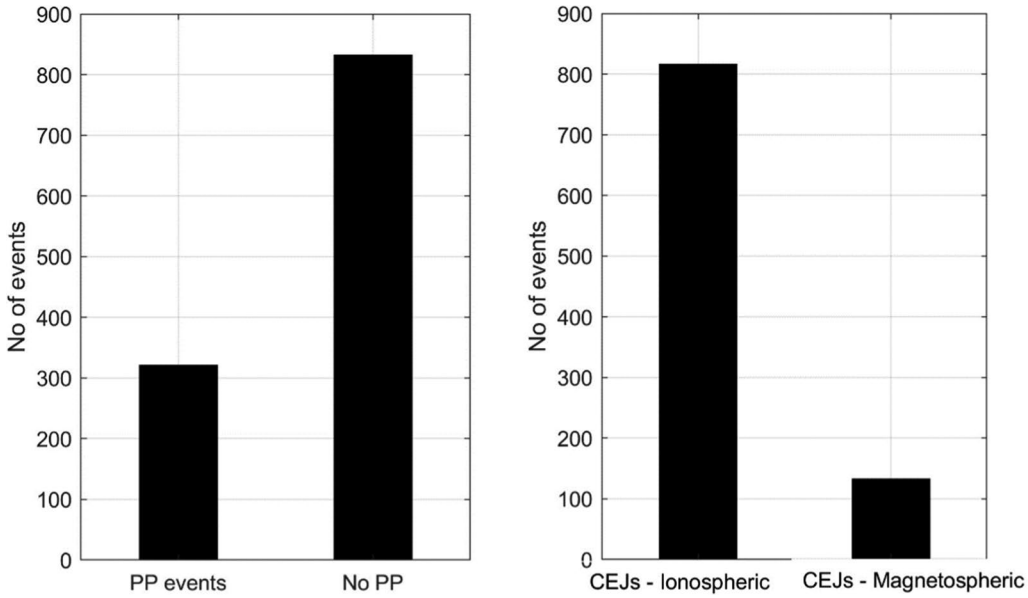

Fig. 10 The total observations from five years of EEJ signature at VEN; total observed PP events; the days where ΔEy shows fluctuations greater than ± 1mVm still not reflected in PP (as No PP); total CEJs which did not correlate with Ey (i.e. ionospheric); the CEJ/PCEJ events which are due to PP at the sites are given

at all three sites, but show substantial differences in amplitudes (Figs. 2, 8 and 9). Figures 6 and 7 indicate that at higher longitudinal separations, the difference in PP amplitudes increases. The number of events with amplitude differences greater than ± 10nT is higher between MNC-CBY (separated at 20°) than between MNC-VEN (separated at 5°) and VEN-CBY (separated at 15°). Additionally, a longitudinal trend of increasing amplitude of PP towards MNC can be observed in Fig. 7. The observed PP amplitude variations from the sites have been reported for all moderate and major storms of 2015 by Bulusu et al. (2018, 2020), and the increase in PP amplitudes towards MNC is attributed to the longitudinal variation of DE3 tide pattern effects of the DE-3. The present study confirms that a longitudinal trend of westward increase of PP amplitudes is evident for both quiet and disturbed times.

The EEJ signal is modified by PP events as well as by westward ionospheric currents, resulting in the formation of CEJs and partial CEJs. The identified CEJs, when the EEJ does not correlate with Ey, are attributed to ionospheric origin mechanisms. However, if the signature of EEJ matches with Ey during the occurrences of CEJs, then it is attributed to magnetospheric/interplanetary origin. From a dataset of five years of EEJ strengths at VEN, it is noted that 133 CEJs (15%) are caused by PP effects (Fig. 10), whereas 816 CEJs (85%) are due to ionospheric origin mechanisms (including disturbance dynamo effects). The analyses in this study have successfully separated CEJs at VEN into ionospheric origin and magnetospheric/interplanetary origin. There are a few events (8%) that show combined effects of ionospheric and interplanetary effects (Fig. 9b), where PP is observed within the CEJ (i.e. the equatorial electric field is already in a westward direction at the site, and the interplanetary electric field signature is reflected in it).

Furthermore, our observations reveal that there are 832 instances of Ey exhibiting significant fluctuations exceeding ± 1 mV/m, yet without causing PP effects. To comprehend the underlying cause behind the absence of PP amidst these intense Ey fluctuations, a thorough investigation is required."

Conclusions

The present study identified the PP events in EEJ of Indian sector using the method suggested by Bulus et al. (2018, 2020). Characteristics of observed PP events studied for both quiet and disturbed period, further longitudinal variability in PP amplitude has been investigated. The influence of interplanetary field disturbances on EEJ and its longitudinal variability have not been specifically addressed in earlier studies, our findings revealed that even during geomagnetically quiet conditions, the interplanetary field can significantly influence EEJ and give rise to CEJ events, which also exhibit longitudinal variations. This has implications for improving the modelling of space weather effects at equatorial stations.

The major findings of the study are as follows:

- *Morphology of PP.* The effects of PP on EEJ exhibit higher efficiency during local noontime hours and for IMF-Bz north directions, both in quiet and disturbed conditions. The variations in PP amplitudes with Ey amplitudes are significantly higher during disturbed conditions for IMF-Bz north, compared to quiet conditions, which supports previous studies. Furthermore, seasonal variations in PP efficiency are observed, with higher efficiency during equinoxes and lower efficiency during solstices in quiet conditions.
- *Perturbations in EEJ by PP.* The CEJs observed during quiet conditions, which correlate well with Ey, confirm that even during geomagnetically quiet conditions, the interplanetary field can significantly influence the equatorial ionospheric currents. The CEJs observed during quiet times that do not correlate with Ey can be attributed to localized ionospheric causal mechanisms. In future studies, these CEJs will be correlated with other ionospheric parameters to further identify the causal phenomena.
- *Spatial variations in PP.* The analysis conducted across three equatorial sites confirms that the amplitudes of PP events vary at short spatial scales, with longitudinal separations of 15-20°. A general longitudinal trend is observed, where PP amplitudes increase towards MNC (westward) compared to CBY (eastward). This trend may be attributed to the influence of the DE-3 tidal structure, where the weaker EEJ at MNC is more susceptible to ionospheric perturbations compared to CBY.

Acknowledgements
This is a CSIR-NGRI contribution with Ref. No: NGRI/Lib/2019/Pub-104 and we thank Director CSIR—NGRI for all support and funding. The authors acknowledge all the public domain data sets CDAWEB and INTERMAGNET for the availability interplanetary and geomagnetic data availability. Additionally, we would like to thank colleagues at the Magnetic Observatory: Dr. Phani Chandrasekhar, K. Chandrasekhar Rao, L. Manjula, and E. Anusha for collection of magnetic data from the remote sites.

Author contributions
First author: computation, analysis, and manuscript writing and scientific discussions. Second author: manuscript suggestions, corrections, and scientific discussions. Third author: concept, manuscript suggestions, corrections, and scientific discussions.

Funding
This work was supported by CSIR-NGRI under MLP-6404-28(KA). Ref. No: NGRI/Lib/2019/Pub-104.

Availability of data and materials
The data for 2015 can be accessed from the following link: http://www.ngri.org.in/upload/kusumita/Kusumita_Data.zip. These data were also used in Archana et al. 2018. Data from HYB are available in INTERMAGNET. Four years of geomagnetic data from VEN will be available upon request at CSIR-NGRI Geomagnetic Observatory, Hyderabad, India.

Declarations

Competing interests
The authors declare that they have no known competing financial interests or personal relationships that could have influenced the work reported in this paper.

Author details
[1]CSIR-National Geophysical Research Institute, Hyderabad, India. [2]Andhra University, Vishakhapatnam, India.

Received: 28 October 2022 Accepted: 30 July 2023
Published online: 14 August 2023

References

Anderson D, Anghel A, Yumoto K, Ishitsuka M, Kudeki E (2002) Estimating daytime vertical *E _ B* drift velocities in the equatorial *F*-region using ground-based magnetometer observations. Geophys Res Lett 29:1596. https://doi.org/10.1029/2001GL014562

Archana RK, Phani Chandrasekhar N, Arora K, Nagarajan N (2018) Constraints on scale lengths of equatorial electrojet and counter electrojet phenomena from the Indian sector. J Geophys Res Space Phys 123:6821–6835. https://doi.org/10.1029/2018JA025213

Bhaskar A, Vichare G (2013) Characteristics of penetration electric fields to the equatorial ionosphere during southward and northward IMF turnings. J Geophys Res Space Phys 118:4696–4709. https://doi.org/10.1002/jgra.50436

Bulusu J, Archana RK, Arora K, Chandrasekhar NP, Nagarajan N (2018) Effect of disturbance electric fields on equatorial electrojet over Indian longitudes. J Geophys Res Space Phys. https://doi.org/10.1029/2018JA025247

Bulusu J, Archana RK, Arora K (2020) Spatial variations in disturbance ionospheric currents-Inference from 12 geomagnetic storms. J Geophys Res-Space Phys. https://doi.org/10.1029/2019JA027718

Earle GD, Kelley MC (1987) Spectral studies of the sources of ionospheric electric fields, J Geophys Res 92(A1): 213–224.

Fejer BG (1986) Equatorial ionospheric electric fields associated with magnetospheric disturbances, in Solar Wind-Magnetosphere Coupling, edited by Kamide Y, and Slavin JA, p. 519–545, Terra Sci, Tokyo.

Fejer BG, Scherliess L (1997) Empirical models of storm time equatorial electric fields, J Geophys Res 102: 24,047.

Fejer BG, Jensen JW, Kikuchi T, Abdu MA, Chau JL (2007) Equatorial Ionospheric Electric Fields During the November 2004 Magnetic Storm. J Geophys Res Space Phys 112(A10). https://doi.org/10.1029/2007JA012376.

Gonzales CA, Kelley MC, Fejer BG, Vickrey JF, Woodman RF (1979) Equatorial electric fields during magnetically disturbed conditions 2. Implications of simultaneous auroral and equatorial measurements, J Geophys Res 84:5803.

Huang C, Foster JC, Kelley MC (2005) Long-duration penetration of the interplanetary electric field to the low-latitude ionosphere during the main phase of magnetic storms. J Geophys Res 110:A11309. https://doi.org/10.1029/2005JA011202

Jaggi RK, Wolf RA (1973) Self-consistent calculation of the motion of a sheet of ions in the magnetosphere. J Geophys Res 78:2852

Kelley MC, Fejer BG, Gonzales CA (1979) An explanation for anomalous ionospheric electric fields associated with a northward turning of the interplanetary magnetic field, Geophys. Res. Lett., 6:301–304. https://doi.org/10.1029/GL006i004p00301.

Kikuchi T, Araki T, Maeda H, Maekawa K (1978) Transmission of polar electric fields to the equator. Nature 273:650–651

Kikuchi T, Araki T (1979) Transient response of uniform ionosphere and preliminary reverse impulse of geomagnetic storm sudden commencement, J Atmos Terr Phys 41:917–925.

Kikuchi T, Lühr H, Kitamura T, Saka O, Schlegel K (1996) Direct penetration of the polar electric field to the equator during a DP 2 event as detected by the auroral and equatorial magnetometer chains and the EISCAT radar. J Geophys Res 101:17161–17173

Kikuchi T, Lühr H, Schlegel K, Tachihara H, Shinohara M, Kitamura T-I (2000) Penetration of auroral electric fields to the equator during a substorm. J Geophys Res 105:23251–23261
Kikuchi T, Hashimoto KK, Kitamura T-I, Tachihara H, Fejer B (2003) Equatorial counter electrojet during substorms. J Geophys Res 108(A11):1406. https://doi.org/10.1029/2003JA009915.
Kpkoska S, Nevison C (1989) Statistical table and formulae. Springer, New York. https://doi.org/10.1007/978-1-4613-9629-1
Manoj C, Maus S, Luhr H, Alken P (2008) Penetration characteristics of the interplanetary electric field to the daytime equatorial ionosphere. J Geophys Res 113:A12310. https://doi.org/10.1029/2008JA013381
Mene NM, Kobéa AT, Obrou OK, Zaka KZ, Boka K, Amory-Mazaudier C, Assamoi P (2011) Statistical study of the DP2 enhancement at the dayside dip-equator compared to low latitudes. Ann Geophys 29:2225–2233. https://doi.org/10.5194/angeo-29-2225-2011
Nishida A (1968) Coherence of geomagnetic *DP* 2 fluctuations with interplanetary magnetic variations. J Geophys Res 73:5549–5559
Nishida A, Iwasaki N, Nagata T (1966) The origin of fluctuations in the equatorial electrojet: a new type of geomagnetic variation. Ann Geophys 22:478–484
Nicolls MJ, Kelley MC, Chau JL, Veliz O, Anderson D, Anghel A (2007) The spectral properties of low latitude daytime electric fields are inferred from magnetometer observations. J Atmos Sol-Terr Phys 69:1160–1173.
Ridley AJ, Liemohn MW (2002) A model-derived storm time asymmetric ring current driven electric field description. J Geophy Res Space Phys 107(A8):SMP 2-1-SMP 2-12. https://doi.org/10.1029/2001JA000051.
Senior C, Blanc M (1984) On the control of magnetospheric convection by the spatial distribution of ionospheric conductivities. J Geophys Res 102(A7):261–284. https://doi.org/10.1029/JA089iA01p00261
Sharma S, Galav P, Dashora N, Alex S, Dabas R. S, Pandey R (2011) Response of low-latitude ionospheric total electron content to the geomagnetic storm of 24 August 2005. J Geophys Res 116:A05317. https://doi.org/10.1029/2010JA016368.
Tsurutani BT, Echer E, Guarnieri FL, Kozyra JU (2008) CAWSES November 7–8, 2004, superstorm: Complex solar and interplanetary features in the post-solar maximum phase. Geophys Res Lett. https://doi.org/10.1029/2007GL031473, in press.
Xiong C, Lühr H, Fejer BG (2016) The response of equatorial electrojet, vertical plasma drift, and thermospheric zonal wind to enhanced solar wind input. J Geophys Res Space Phys 121:5653–5663. https://doi.org/10.1002/2015JA022133

Publisher's Note